3D Ion percolation path in gadolinium doped ceria nanofibres for solid oxide electrochemical cells

Colding-Fagerholt, Sofie; Simonsen, Søren Bredmose; Jørgensen, Peter Stanley; Zhang, Wenjing; Huang, Xiaoxu; Schmidt, Søren; Kuhn, Luise Theil

Published in:
Scripta Materialia

Link to article, DOI:
10.1016/j.scriptamat.2025.116545

Publication date:
2025

Document Version
Publisher's PDF, also known as Version of record

Scripta Materialia 259 (2025) 116545

Contents lists available at ScienceDirect

Scripta Materialia

journal homepage: www.journals.elsevier.com/scripta-materialia

3D Ion percolation path in gadolinium doped ceria nanofibres for solid oxide electrochemical cells

Sofie Colding-Fagerholt [a], Søren Bredmose Simonsen [a,*], Peter Stanley Jørgensen [a], Wenjing Zhang [b], Xiaoxu Huang [c], Søren Schmidt [d,e], Luise Theil Kuhn [a]

[a] DTU Energy, Technical University of Denmark, Fysikvej, 2800 Kgs. Lyngby, Denmark
[b] DTU Environment, Technical University of Denmark, Bygningstorvet, 2800 Kgs. Lyngby, Denmark
[c] DTU Mechanical Engineering, Technical University of Denmark, Produktionstorvet 427, 2800 Kgs. Lyngby, Denmark
[d] DTU Physics, Technical University of Denmark, Fysikvej, 2800 Kgs. Lyngby, Denmark
[e] European Spallation Source ERIC, Data Management and Software Centre, Asmussens Allé 305, 2800 Lyngby Denmark

ARTICLE INFO

Keywords:
3D orientation mapping
Transmission electron microscope
Solid oxide electrochemical cells
Electrospun nanofibres
Ion percolation path

ABSTRACT

Understanding transport properties in ion conductive solids is key to supporting the development of devices for energy conversion, e.g., solid oxide electrochemical cells. Because of the complex nanostructured nature of such materials they have numerous types of grain boundaries and the prediction of the percolation path becomes challenging. We employ, for the first time, a combination of 3D orientation mapping in the transmission electron microscope and energy filtered transmission electron microscopy to map crystal orientation and doping concentration with nm-precision to predict 3D ion percolation paths in state-of-the-art electrospun ($Ce_{0.9}Gd_{0.1}O_{1.95}$) nanofibres. The results show that the conductivity of CGO nanofibres are affected by grain- and diameter size. Furthermore, we show that 3D-OMiTEM is a powerful non-destructive tool for determining 3D ion percolation paths with nm-precision of complex nanostructures.

An increasing interest in the use of renewable energy sources emphasizes the need for high performance energy conversion devices. Examples of such devices include, but are not restricted to, Solid Oxide Electrolysis Cells (SOECs) and Fuel Cells (SOFCs) [1].

Solid Oxide Cells (SOC) are composed of electronic-, ionic- and mixed conductors and high conductivity is an important property for optimal performance. To develop and optimize such devices it is critical to understand the charge transport properties in ion conductive solids [2,3].

The ionic and electronic conductivity of functional materials, used in SOCs, are closely related to the nano- and micro-granular structure since they contain a large fraction of grain boundaries (GB) [2–9]. It is widely accepted that the ionic conductivity in the interior of the grains are orders of magnitude larger than at the GB and as a result, the GBs often become the limiting factor for obtaining a higher conductivity [4–9]. The conductivity in the GB is determined by equation 1 [3,4].

$$\sigma_{GB} = \beta_{GB}\frac{n_v^{GB}}{T}exp\left(\frac{-E^{GB}}{kT}\right), \quad (1)$$

where σ_{GB} is the GB conductivity, β_{GB} is the pre-exponential conductivity, which is independent of the doping-concentration, n_v^{GB} is the effective GB carrier concentration, i.e. the average concentration of oxygen vacancies in a GB, k is the Boltzmann factor, T is the temperature and E^{GB} is the GB activation energy.

The pre-exponential factor has been widely studied [10–17]. However, the activation energy is difficult to determine as it depends on the composition of the individual GB. The complex nano-structured nature of the materials generates a variety of possible GB-types with different atomic structures and compositions. This makes it challenging to fully understand the fundamentals and parameters affecting the overall performance.

A recent study by Bowman et al. (2020) has gathered literature [11–17] on the field to determine the activation energy as a function of GB doping concentration for gadolinium doped ceria (CGO). By fitting the data empirically, they determined the relationship in Eq. (2) [3],

$$E^{GB} = 2{\cdot}10^{-4}\left(\left[A^{3+}\right]_{GB}\right)^{-5} + 0.91, \quad (2)$$

* Corresponding author
E-mail address: sobrs@dtu.dk (S.B. Simonsen).

https://doi.org/10.1016/j.scriptamat.2025.116545
Received 31 October 2024; Received in revised form 3 January 2025; Accepted 6 January 2025
Available online 11 January 2025

where $[A^{3+}]_{GB}$ is the trivalent doping concentration.

The study by Bowman et al. (2020) furthermore suggests a linear relationship between the crystalline misorientation angle of two neighbouring grains and the GB doping concentration [3]. This gives the opportunity to determine the local GB doping concentration, and thereby the GB- activation energy and conductivity, directly from a crystal orientation map. Hence, a crystal orientation map will be able to predict possible ion percolation paths, which could help determine the overall conductivity of the sample.

The overall conductivity can be affected by cracks or other structural changes [18]. Therefore, the 3D ion percolation path would be a valuable contribution to understanding the fundamentals of ion conductive solids.

3D orientation mapping in the transmission electron microscope (OMiTEM) is a promising technique for non-destructive visualization the 3D orientation of nanocrystals. Liu et al. first described the method applied on a simulated data set and on an aluminium thin foil in 2011 [19]. More recently Wu et al. (2020) has described the method applied on a gold nano-island film and on lattice rotations in nanograined Ni [20,21].

In the present work, we apply OMiTEM on a functional material, namely electro-spun CGO nanofibres. Such nanofibres have recently shown potential for application in SOCs [22–27]. By combining 3D crystal orientation maps from the OMiTEM data with energy filtered transmission electron microscopy (EFTEM). From this, ion percolation paths with lowest resistivity was calculated and visualized. To the best of our knowledge, percolation paths with such high resolution in 3D has not been reported in previous works. The details of this work is described in the following.

OMiTEM was applied on CGO electrospun nanofibres calcined at 800 °C for 1 and for 10 h, respectively, in atmospheric air. Using in-house developed software, the grain positions and orientations are reconstructed resulting in a multi-dimensional data set with x, y and z coordinates, each with a confidence index and crystal orientation. The results are shown on Fig. 1.

The orientation maps show the electrospun fibres in 3D with grains coloured by their crystal orientation in inverse pole figure (IPF) color (Fig. 1). The individual grains are defined as well as the overall morphological structure of the fibre. This enables extraction of geometric and orientation parameters of all grains for statistical analysis. The geometric analysis showed that the sample calcined for 1 hour has a mean diameter of 29.9 ± 0.9 nm and after 10 h it increased to 35.3 ± 1.6 nm, i.e. an 18 % increase. The orientation analysis showed that the fibres have a random isotropic distribution and are thus indistinguishable with regards to crystal orientation distribution (for further information see supporting information S2, S3 and figure S1, S2 and S2). To our knowledge this is the first time this type of 3D analysis has been conducted on electrospun nano fibres.

From orientation maps, statistical as well as local information, can be obtained and this provides new possibilities for extracting information about nano-structured materials. In the following sections we demonstrate some of the possibilities.

The misorientation of grains can be used to find the local GB doping concentration, as described in the work by Bowman et al. [3]. To find the relationship between the misorientation and the doping concentration, EFTEM atomic ratio mapping as described in[28,29] was acquired (Fig. 2a) followed by OMiTEM (Fig. 2b) of the same flat area (for further information see supporting info section S6 and figure S5 and figure S6).

The result is shown of Fig. 2c and the linear relationship, in Eq. (3), was determined from the fit in good agreement with Bowman et al. (2020) [3].

$$\left[A^{+3}\right] = 8{\cdot}10^{-2} + 4{\cdot}10^{-3}{\cdot}m \tag{3}$$

In Eq. (3), m denotes the crystallographic misorientation angle (deg) of neighbouring grains. The EFTEM result furthermore revealed that at the surface the gadolinium content was the same as that of a GB with approximately 62° misorientation, which is the highest for a cubic structure.

From the local doping concentration, the activation energy and thereby the resistivity can be mapped using Eqs. (1), (2) and (3). A slice through the middle of the calculated resistivity map, is shown on Fig. 3c and 3d. Here the grain interior has been assigned with the value of $\rho = 1 \cdot 10^3$ Ω cm as in[4] at 440 °C.

A possible ion percolation path is obtained by locating the path with

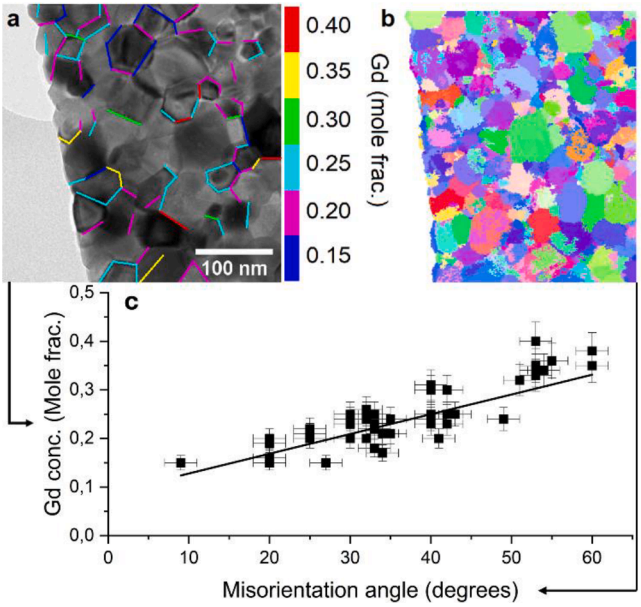

Fig. 2. Relationship between grain boundary doping concentration and misorientation angle of neighbouring grains. a shows the result of the EFTEM atomic ratio mapping where the results of the gadolinium ratio are overlaid a BF-image. b is the corresponding orientation map and c is the graph correlating the grain boundary doping concentration with the misorientation angle of neighbouring grains.

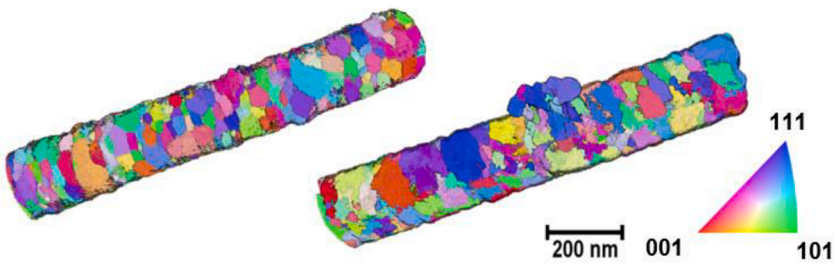

Fig. 1. Orientation maps of elctrospun CGO fibre calcined at 800 °C. Left: calcined for 1 hour. Right: calcined for 10 h. The colours are inverse pole figure (IPF) colouring showing crystal directions.

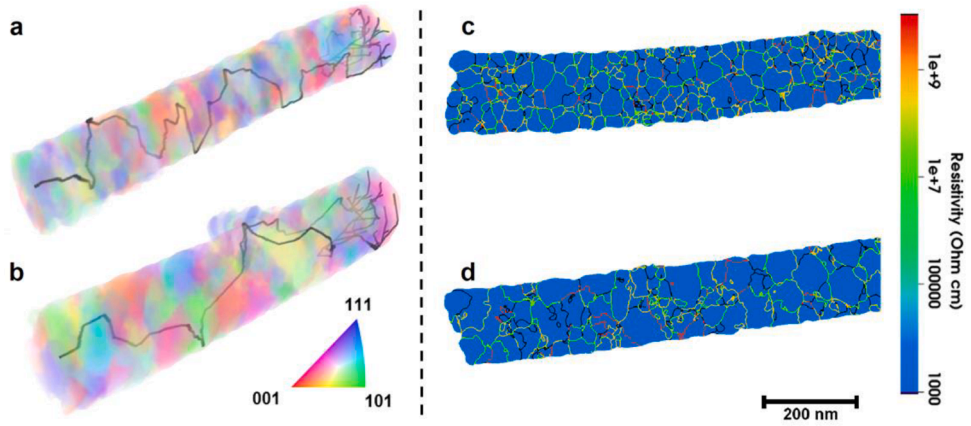

Fig. 3. Visualization of percolation path and resistivity. a and c show the structure of a CGO nanofibre calcined at 800 °C for 1 hour, b and d is the structure of a CGO nanofibre calcined at 800 °C for 10 hour. a and b is the 3D visualization including the percolation path. The black path represents the ion percolation path with the smallest resistance. The colors are IPF colors visualizing different orientations. c and d shows a slice through the middle of the sample revealing the calculated resistivity at 440 °C. The grain interior has been assign with the value of $\rho = 10^3$ Ω·cm. The colors represent the resistivity in the structure.

the lowest resistivity in the fibre. This is done by distributing starting points evenly at the end of the fibre. Furthermore, the surface resistivity was set to have the value as at a GB with 62° misorientation as found by EFTEM. The obtained percolation path is presented in Fig. 3a and 3b.

Fig. 3a and 3b, to our knowledge, demonstrates for the first time the percolation path at such high resolution in 3D. With the 3D information it is possible to determine the percolation path with minimum resistance. This is done for the entire 3D structure and not just for a 2D slice.

As presented above, the two CGO fibres have different mean grain sizes, and the relationship between conductivity and grain size can therefore established. To also predict the relation between conductivity and fibre diameter, we stepwise virtually shrink the nanofibre diameters by removing voxels from the surfaces. The results on Fig. 4 show a) that the effective resistivity decreases with increasing mean grain size and b) that the effective resistivity of the percolation path increases as the fibre becomes smaller, with a more rapid increase as the fibre diameter approaches zero. This is a consequence of the fibre containing fewer grains and GBs as its diameter diminishes, leading to an increased probability of the percolation path having to cross a GB with high resistance or having to travel on the surface. The onset of the more rapid increase in resistivity can be seen to occur at small fibre diameters (< 20 nm). This corresponds roughly to when we would expect the fibre cross section to only contain a single grain. With no alternatives for less resistive GBs the percolation path must pass the present GB even at a high resistance i.e. the rapid increase corresponds to a change from few alternative GBs to no alternative GBs.

The percolation path in the CGO fibre calcined for 10 h is seen to have a significantly lower effective resistivity than the CGO fibre calcined for 1 hour ($3.49 \cdot 10^5$ Ω·cm vs. $6.06 \cdot 10^5$ Ω·cm). The main contribution to the resistance in the percolation path comes from crossing GBs rather than the bulk CGO resistivity. The increased effective resistivity in the CGO fibre calcined for 1 hour can thus be explained by the smaller grain size, leading to an additional number of GBs to be crossed in the percolation path.

Our study reveals that OMiTEM is a feasible tool to non-destructively visualize crystal orientation in polycrystalline nanofibres in 3D. The results showed that CGO1 and CGO10 are indistinguishable with regards to the global crystal orientation distribution and only the mean grain size separates them. The analysis of the fibres shows that the conductivity of the nanofibres are influenced by the grain sizes and fibre diameters via variations in the percolation paths.

The work offers an insight into the possibilities of OMiTEM. OMiTEM can be used to gain 3D orientation information locally on the entire sample enabling orientation- and structural analysis which ultimately

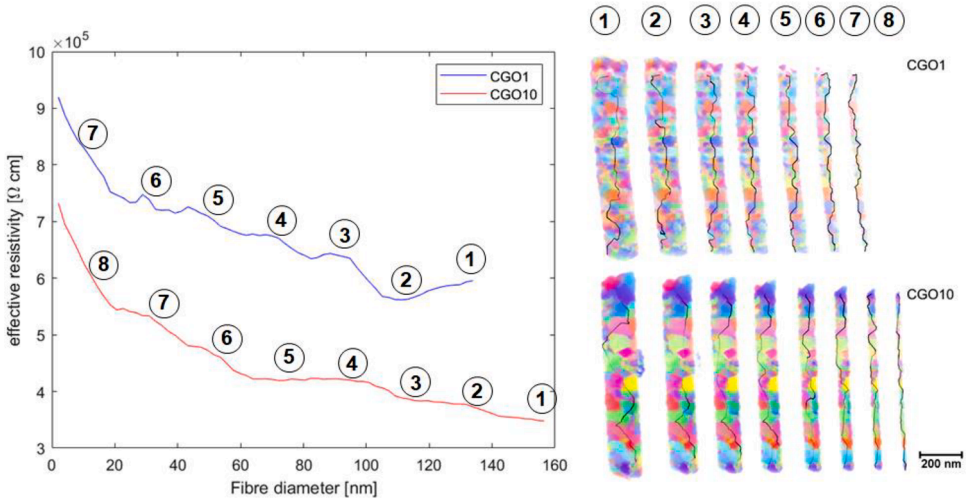

Fig. 4. Left: Percolation path resistivity as a function of fibre diameter at the narrowest point on the fibre for the CGO calcined for 1 hour and CGO calcined for 10 h. The largest plotted fibre diameter corresponds to the unaltered fibre before erosion. Right: 3D recocnstruction of erroded CGO fibre calcined for 1 hour and 10 h. Numbers indicate the position on the graph.

can predict possible ion percolation paths. This can prove to be a powerful tool to understand the fundamentals of GBs in solid oxide cells and a step closer to understanding pathways in polycrystalline solids to support the development and optimization of devices for energy conversion.

Supporting Information Available

Materials and Methods; Orientation Analysis; Size distribution and Evaluation of 3DOMiTEM; Assessment of beam damage; Missing wedge effect; EFTEM analysis; Determination of Percolation Path with Least Resistivity; Figures S1 to S6

CRediT authorship contribution statement

Sofie Colding-Fagerholt: Writing – original draft, Visualization, Validation, Investigation, Formal analysis, Data curation. **Søren Bredmose Simonsen:** Writing – review & editing, Validation, Supervision, Conceptualization. **Peter Stanley Jørgensen:** Writing – review & editing, Validation, Investigation, Formal analysis. **Wenjing Zhang:** Writing – review & editing, Supervision, Resources, Methodology. **Xiaoxu Huang:** Writing – review & editing, Methodology. **Søren Schmidt:** Writing – review & editing, Validation, Supervision, Methodology, Conceptualization. **Luise Theil Kuhn:** Writing – review & editing, Validation, Supervision, Resources, Project administration, Funding acquisition, Conceptualization.

Declaration of competing interest

The authors declare that they have no known competing financial interests or personal relationships that could have appeared to influence the work reported in this paper.

Acknowledgement

The authors thank Peter A. Crozier for the fruitful discussions and Rune E. Johnsen for assisting with X-Ray Diffraction measurements.

Supplementary materials

Supplementary material associated with this article can be found, in the online version, at doi:10.1016/j.scriptamat.2025.116545.

References

[1] N.Q. Minh, Solid oxide fuel cell technology - Features and applications, Solid. State Ion. 174 (2004) 271–277.
[2] S.H. Jo, P. Muralidharan, D.K. Kim, Electrical characterization of dense and porous nanocrystalline Gd-doped ceria electrolytes, Solid. State Ion. 178 (2008) 1990–1997.
[3] W.J. Bowman, A. Darbal, P.A. Crozier, Linking macroscopic and nanoscopic ionic conductivity: a semiempirical framework for characterizing grain boundary conductivity in polycrystalline ceramics, ACS Appl. Mater. Interf. 12 (2020) 507–517.
[4] W.J. Bowman, M.N. Kelly, G.S. Rohrer, C.A. Hernandez, P.A. Crozier, Enhanced ionic conductivity in electroceramics by nanoscale enrichment of grain boundaries with high solute concentration, Nanoscale 9 (2017) 17293–17302.
[5] R.A. De Souza, J. Fleig, J. Maier, Z. Zhang, W. Sigle, M. Rühle, Electrical resistance of low-angle tilt grain boundaries in acceptor-doped $SrTiO_3$ as a function of misorientation angle, J. Appl. Phys. (2005) 97.
[6] R. Waser, Electronic properties of grain boundaries in $SrTiO_3$ and $BaTiO_3$ ceramics, Solid. State Ion. 75 (1995) 89–99.
[7] D.Y. Wang, A.S. Nowick, The "grainboundary effect" in doped ceria solid electrolytes, J. Solid. State Chem. 35 (1980) 325–333.
[8] J. Tanaka, J. Baumard, P. Abelard, Nonlinear electrical-properties of grainboundaries in an oxygen-ion conductor ($CeO_2Y_2O_3$), J. American Ceram. Soc. 70 (1987) 637–643.
[9] F. Ye, C.Y. Yin, D.R. Ou, T. Mori, Relationship between lattice mismatch and ionic conduction of grain boundary in YSZ, Prog. Natural Sci. Mater. Int 24 (2014) 83–86.
[10] T. Zhang, Z. Zeng, H. Huang, P. Hing, J. Kilner, Effect of alumina addition on the electrical and mechanical properties of $Ce_{0.8}Gd_{0.2}O_{2-\delta}$ ceramics, Mater. Lett. 57 (2002) 124–129.
[11] W.J. Bowman, J. Zhu, R. Sharma, P.A. Crozier, Electrical conductivity and grain boundary composition of Gd-doped and Gd/Pr co-doped ceria, Solid. State Ion. 272 (2015) 9–17.
[12] H.J. Avila-Paredes, K. Choi, C.T. Chen, S. Kim, Dopantconcentration dependence of grainboundary conductivity in ceria: a space-charge analysis, J. Mater. Chem. 19 (2009) 4837–4842.
[13] R. Gerhardt, A.S. Nowick, Grain-boundary effect in ceria doped with trivalent cations: i, electrical measurements, J. American Cera. Soc. 69 (1986) 641–646.
[14] A. Jasper, J.A. Kilner, D.W. McComb, TEM and impedance spectroscopy of doped ceria electrolytes, Solid. State Ion. 179 (2008) 904–908.
[15] T.S. Zhang, J. Ma, H. Cheng, S.H. Chan, Ionic conductivity of highpurity Gd-doped ceria solid solutions, Mater. Res. Bull. 41 (2006) 563–568.
[16] H.J. Avila-Paredes, S. Kim, The effect of segregated transition metal ions on the grain boundary resistivity of gadolinium doped ceria: alteration of the space charge potential, Solid. State Ion. 177 (2006) 3075–3080.
[17] G.M. Christie, F.P. Van Berkel, Microstructure - Ionic conductivity relationships in ceria-gadolinia electrolytes, Solid. State Ion. 83 (1996) 17–27.
[18] S. De Angelis, P.S. Jørgensen, V. Esposito, E. Hsiao Rho Tsai, M. Holler, K. Kreka, E. Abdellahi, J.R Bowen, Ex situ tracking solid oxide cell electrode microstructural evolution in a redox cycle by high resolution ptychographic nanotomography, J. Power. Sources. 360 (2017) 520–527.
[19] H.H. Liu, S. Schmidt, H.F. Poulsen, A. Godfrey, Z.Q. Liu, J.A. Sharon, X. Huang, Three-dimensional orientation mapping in the transmission electron microscope, Science (1979) 332 (2011) 833–834.
[20] G. Wu, W. Zhu, Q. He, Z. Feng, T. Huang, L. Zhang, S. Schmidt, A. Godfrey, X. Huang, 2D and 3D orientation mapping in nanostructured metals: a review, Nano Mater Sci. 2 (2020) 50–57.
[21] Q. He, S. Schmidt, W. Zhu, G. Wu, T. Huang, L. Zhang, D.J. Jensen, Z. Feng, A. Godfrey, X. Huand, 3D microscopy at the nanoscale reveals unexpected lattice rotations in deformed nickel, Science (1979) 382 (2023) 1065–1069.
[22] M. Zhi, S. Lee, N. Miller, N.H. Menzler, N. Wu, An intermediate temperature solid oxide fuel cell with electrospun nanofiber cathode, Ener. Environm. Sci 5 (2012) 7066–7071.
[23] E. Zhao, Z. Jia, L. Zhao, Y. Xiong, C. Sun, M.E. Brito, One dimensional $La_{0.8}Sr_{0.2}Co_{0.2}Fe_{0.8}O_{3-\delta}Ce_{0.8}Gd_{0.2}O_{1.9}$ nanocomposite cathodes for intermediate temperature solid oxide fuel cells, J. Power. Sources. 219 (2012) 133–139.
[24] C.C. Chou, C.F. Huang, T.H. Yeh, Characterization and catalytic activity of $La_{0.6}Sr_{0.4}Co_{0.2}Fe_{0.8}O_3$-yttria stabilized zirconia electrospun nano-fiber as a cathode catalyst, Ceram. Int. 39 (2013) S549–S553.
[25] L. Li, P. Zhang, R. Liu, S.M. Guo, Preparation of fibrous Ni-coated-YSZ anodes for solid oxide fuel cells, J. Power. Sources. 196 (2011) 1242–1247.
[26] L. Fan, Y. Xiong, L. Liu, Y. Wang, H. Kishimoto, K. Yamaji, T. Horita, Performance of $Gd_{0.2}Ce_{0.8}O_{1.9}$ infiltrated $La_{0.2}Sr_{0.8}TiO_3$ nanofiber scaffolds as anodes for solid oxide fuel cells, J. Power. Sources. 265 (2014) 125–131.
[27] Zhang, W. Electrospinning for solid oxide fuel cells. In *electrospinning for advanced energy and environmental applications* 2015, 61–76.
[28] F. Hofer, W. Grogger, G. Kothleitner, P. Warbichler, Quantitative analysis of EFTEM elemental distribution images, Ultramicroscopy. 67 (1997) 83–103.
[29] P. Thomas, P. Midgley, EFTEM, Transmiss. Electron Micros. (2016) 377–404.